Physics Letters B 770 (2017) 193–199

Contents lists available at ScienceDirect

Physics Letters B

www.elsevier.com/locate/physletb

The frozen nucleon approximation in two-particle two-hole response functions

I. Ruiz Simo [a], J.E. Amaro [a,*], M.B. Barbaro [b], J.A. Caballero [c], G.D. Megias [c], T.W. Donnelly [d]

[a] Departamento de Física Atómica, Molecular y Nuclear, and Instituto de Física Teórica y Computacional Carlos I, Universidad de Granada, Granada 18071, Spain
[b] Dipartimento di Fisica, Università di Torino and INFN, Sezione di Torino, Via P. Giuria 1, 10125 Torino, Italy
[c] Departamento de Física Atómica, Molecular y Nuclear, Universidad de Sevilla, Apdo.1065, 41080 Sevilla, Spain
[d] Center for Theoretical Physics, Laboratory for Nuclear Science and Department of Physics, Massachusetts Institute of Technology, Cambridge, MA 02139, USA

ARTICLE INFO

Article history:
Received 3 March 2017
Received in revised form 21 April 2017
Accepted 24 April 2017
Available online 27 April 2017
Editor: W. Haxton

Keywords:
Neutrino scattering
Meson-exchange currents
2p–2h

ABSTRACT

We present a fast and efficient method to compute the inclusive two-particle two-hole (2p–2h) electroweak responses in the neutrino and electron quasielastic inclusive cross sections. The method is based on two approximations. The first neglects the motion of the two initial nucleons below the Fermi momentum, which are considered to be at rest. This approximation, which is reasonable for high values of the momentum transfer, turns out also to be quite good for moderate values of the momentum transfer $q \gtrsim k_F$. The second approximation involves using in the "frozen" meson-exchange currents (MEC) an effective Δ-propagator averaged over the Fermi sea. Within the resulting "frozen nucleon approximation", the inclusive 2p–2h responses are accurately calculated with only a one-dimensional integral over the emission angle of one of the final nucleons, thus drastically simplifying the calculation and reducing the computational time. The latter makes this method especially well-suited for implementation in Monte Carlo neutrino event generators.

1. Introduction

The analysis of modern accelerator-based neutrino oscillation experiments requires good control over the intermediate-energy neutrino-nucleus scattering cross section [1,2]. In particular the importance of multi-nucleon events has been suggested in many calculations of charge-changing quasielastic cross sections (ν_μ, μ), at typical neutrino energies of $\sim$1 GeV [3–9]. The contribution of two-particle–two-hole (2p–2h) excitations is now thought to be essential for a proper description of data [10–19]. Thus a growing interest has arisen in including 2p–2h models into the Monte Carlo event generators used by the neutrino collaborations [20–23].

The only 2p–2h model implemented up to date in some of the Monte Carlo neutrino event generators corresponds to the so-called 'IFIC Valencia model' [6,9], which has been incorporated in GENIE, NuWRO and NEUT [24–26]. There are also plans to incorporate the 'Lyon model' [3] in GENIE, while phenomenological approaches like the effective transverse enhancement model of [27] are implemented, for instance, in NuWro generator [25].

One of the main problems to implementing the 2p–2h models is the high computational time. This is due to the large number of nested integrals involved in the evaluation of the inclusive hadronic tensor with sums over the final 2p–2h states. To speed up the calculations, several approximations can be made, such as choosing an average momentum for the nucleons in the local Fermi gas [6], neglecting the exchange matrix elements, or reducing the number of integrations to two nested integrals by performing a non-relativistic expansion of the current operators [28]. The latter approach is only useful for some pieces of the elementary 2p–2h response.

In this work we present a fast and very efficient method to calculate the inclusive 2p–2h responses in the relativistic Fermi gas model (RFG). This approach, denoted as the frozen nucleon approximation, was first explored in [29] but restricted to the analysis of the 2p–2h phase-space. Here it is extended to the evaluation of the full hadronic tensor assuming that the initial momenta of the two struck nucleons can be neglected for high enough energy and momentum transfer, $q > k_F$. The frozen nucleon approximation was found to work properly in computing the phase space function for two-particle emission in the range of momentum transfers of interest for neutrino experiments with accelerators. Here we investigate

* Corresponding author.
E-mail addresses: ruizsig@ugr.es (I. Ruiz Simo), amaro@ugr.es (J.E. Amaro).

http://dx.doi.org/10.1016/j.physletb.2017.04.063

the validity of the frozen approximation beyond the phase-space study by including the electroweak meson-exchange current (MEC) model of [30]. We find that the presence of virtual delta excitations requires one to introduce a "frozen" Δ-propagator, designed by a convenient average over the Fermi sea.

The main advantage of the frozen approximation consists in reducing the number of nested integrals needed to evaluate the inclusive 2p–2h electroweak responses from 7 (full calculation) to 1. Thus it is well-suited to computing the 2p–2h neutrino cross sections folded with the neutrino flux, and it can be of great help in order to implement the 2p–2h models in the Monte Carlo codes currently available.

The plan of this work is as follows: in section 2 we review the formalism of neutrino scattering and describe mathematically the frozen approximation approach. In section 3 we validate the nucleon frozen approximation by computing the 2p–2h response functions and by comparing with the exact calculation. Finally, in section 4 we summarize our conclusions.

2. Formalism

2.1. Cross section and hadronic tensor

The double-differential inclusive (ν_l, l^-) or $(\bar{\nu}_l, l^+)$ cross section is given by

$$\frac{d^2\sigma}{d\Omega' d\epsilon'} = \sigma_0 \Big[\widetilde{V}_{CC} R^{CC} + 2\widetilde{V}_{CL} R^{CL} + \widetilde{V}_{LL} R^{LL} + \widetilde{V}_T R^T \pm 2\widetilde{V}_{T'} R^{T'} \Big], \tag{1}$$

where the sign ± is positive for neutrinos and negative for antineutrinos. The term σ_0 in Eq. (1) represents the elementary neutrino scattering cross section with a point nucleon, while the $\widetilde{V}_K$ are kinematic factors that depend on lepton kinematic variables. Their explicit expressions can be found in [31]. The relevant nuclear physics is contained in the five nuclear response functions $R^K(q,\omega)$, where $\mathbf{q}$ is the momentum transfer, defining the z direction, and ω is the energy transfer. They are defined as suitable combinations of the hadronic tensor

$$R^{CC} = R^L = W^{00} \tag{2}$$

$$R^{CL} = -\frac{1}{2}\left(W^{03} + W^{30}\right) \tag{3}$$

$$R^{LL} = W^{33} \tag{4}$$

$$R^T = W^{11} + W^{22} \tag{5}$$

$$R^{T'} = -\frac{i}{2}\left(W^{12} - W^{21}\right). \tag{6}$$

In this work we compute the inclusive hadronic tensor for two-nucleon emission in the relativistic Fermi gas, given by

$$W^{\mu\nu}_{\text{2p-2h}} = \frac{V}{(2\pi)^9} \int d^3p'_1 d^3h_1 d^3h_2 \frac{m_N^4}{E_1 E_2 E'_1 E'_2} \times r^{\mu\nu}(\mathbf{p}'_1, \mathbf{p}'_2, \mathbf{h}_1, \mathbf{h}_2)\, \delta(E'_1 + E'_2 - E_1 - E_2 - \omega) \times \Theta(p'_1, p'_2, h_1, h_2), \tag{7}$$

where $\mathbf{p}'_2 = \mathbf{h_1} + \mathbf{h_2} + \mathbf{q} - \mathbf{p}'_1$ by momentum conservation, m_N is the nucleon mass, V is the volume of the system and we have defined the product of step functions

$$\Theta(p'_1, p'_2, h_1, h_2) = \theta(p'_2 - k_F)\theta(p'_1 - k_F)\theta(k_F - h_1)\theta(k_F - h_2) \tag{8}$$

with k_F the Fermi momentum.

Finally the function $r^{\mu\nu}(\mathbf{p}'_1, \mathbf{p}'_2, \mathbf{h}_1, \mathbf{h}_2)$ is the elementary hadron tensor for the 2p–2h transition of a nucleon pair with given initial and final momenta, summed up over spin and isospin,

$$r^{\mu\nu}(\mathbf{p}'_1, \mathbf{p}'_2, \mathbf{h}_1, \mathbf{h}_2) = \frac{1}{4}\sum_{s,t} j^\mu(1',2',1,2)^*_A j^\nu(1',2',1,2)_A, \tag{9}$$

which is written in terms of the antisymmetrized two-body current matrix elements

$$j^\mu(1',2',1,2)_A \equiv j^\mu(1',2',1,2) - j^\mu(1',2',2,1). \tag{10}$$

The factor 1/4 in Eq. (9) accounts for the antisymmetry of the two-body wave function.

For the inclusive responses considered in this work there is a global axial symmetry, so we can fix the azimuthal angle of one of the particles. We choose $\phi'_1 = 0$, and consequently the integral over ϕ'_1 gives a factor 2π. Furthermore, the energy delta function enables analytical integration over p'_1, and so the integral in Eq. (7) can be reduced to 7 dimensions (7D). In the "exact" results shown in the next section, this 7D integral has been computed numerically using the method described in [29].

2.2. Frozen nucleon approximation

The frozen nucleon approximation consists in assuming that the momenta of the initial nucleons can be neglected for high enough values of the momentum transfer. Thus, in the integrand of Eq. (7), we set $\mathbf{h}_1 = \mathbf{h}_2 = 0$, and $E_1 = E_2 = m_N$. We roughly expect this approximation to become more accurate as the momentum transfer increases. The integration over $\mathbf{h}_1, \mathbf{h}_2$ is trivially performed and the response function R^K, with $K = CC, CL, LL, T, T'$, is hence approximated by

$$R^K_{\text{frozen}} = \frac{V}{(2\pi)^9}\left(\frac{4}{3}\pi k_F^3\right)^2 \int d^3p'_1 \frac{m_N^2}{E'_1 E'_2} r^K(\mathbf{p}'_1, \mathbf{p}'_2, \mathbf{0}, \mathbf{0}) \times \delta(E'_1 + E'_2 - 2m_N - \omega)\, \Theta(p'_1, p'_2, 0, 0), \tag{11}$$

where $\mathbf{p}'_2 = \mathbf{q} - \mathbf{p}'_1$ and r^K are the elementary response functions for a nucleon pair excitation, which are defined similarly to Eqs. (2)–(6). The integral over p'_1 can be done analytically by using the delta function for energy conservation, and the integral over ϕ'_1 gives again a factor of 2π. Thus only an integral over the polar angle θ'_1 remains:

$$R^K_{\text{frozen}} = \frac{V}{(2\pi)^9}\left(\frac{4}{3}\pi k_F^3\right)^2 2\pi \int_0^\pi d\theta'_1 \sin\theta'_1 \times \sum_{\alpha=\pm} \frac{m_N^2 {p'_1}^2 \Theta(p'_1, p'_2, 0, 0)}{E'_1 E'_2 \left|\frac{p'_1}{E'_1} - \frac{\mathbf{p}'_2 \cdot \widehat{\mathbf{p}}'_1}{E'_2}\right|} r^K(\mathbf{p}'_1, \mathbf{p}'_2, \mathbf{0}, \mathbf{0})\Big|_{p'_1 = p'^{(\alpha)}_1} \tag{12}$$

where the sum runs over the, in general two, possible values of the momentum of the first particle for given emission angle θ'_1. These are obtained as the positive solutions ${p'_1}^{(\pm)}$ of the energy conservation equation

$$2m_N + \omega = \sqrt{{p'_1}^2 + m_N^2} + \sqrt{(\mathbf{q} - \mathbf{p}'_1)^2 + m_N^2}. \tag{13}$$

The explicit values of the solutions of the above equation can be found in the appendix of [29]. Care is needed in performing the integral over θ'_1 because the denominator inside the integral can be zero for some kinematics. The quadrature in these cases can be done with the methods explained in [29,32].

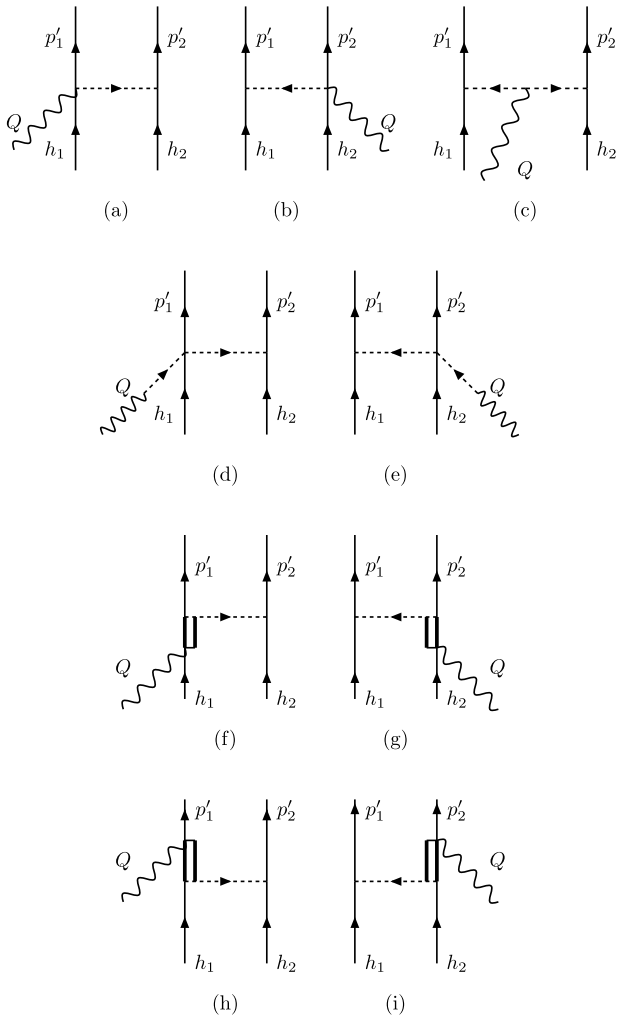

Fig. 1. Feynman diagrams for the electroweak MEC model used in this work.

2.3. Electroweak meson-exchange currents

To investigate the validity of the frozen nucleon approximation, we have to choose a specific model for the two-body current matrix elements $j^\mu(1',2',1,2)$ entering in the elementary 2p–2h response functions, Eqs. (9), (10). Here we use the relativistic model of electroweak MEC operators developed in [30]. The MEC model can be summarized by the Feynman diagrams depicted in Fig. 1. It comprises several contributions coming from the pion production amplitudes of [33].

The Seagull current, corresponding to diagrams (a,b), is given by the sum of vector and axial-vector pieces

$$j^\mu_{\rm sea} = \left[I^\pm_V\right]_{1'2',12} \frac{f^2_{\pi NN}}{m^2_\pi} \frac{\bar u_{s'_1}(\mathbf{p}'_1)\,\gamma_5 \not{k}_1\, u_{s_1}(\mathbf{h}_1)}{k_1^2 - m_\pi^2} \times \bar u_{s'_2}(\mathbf{p}'_2)\left[F_1^V(Q^2)\gamma_5\gamma^\mu + \frac{F_\rho\left(k_2^2\right)}{g_A}\gamma^\mu\right] u_{s_2}(\mathbf{h}_2) + (1\leftrightarrow 2)\,, \tag{14}$$

where $I^\pm_V = (I_V)_x \pm i(I_V)_y$ corresponds to the $\pm$-components of the two-body isovector operator $\boldsymbol{I}_V = i[\boldsymbol{\tau}(1)\times\boldsymbol{\tau}(2)]$. The $+(-)$ sign refers to neutrino (antineutrino) scattering. The four-vector $k_1^\mu = (p'_1 - h_1)^\mu$ is the momentum carried by the exchanged pion and $Q^\mu = (\omega, \mathbf{q})$. The πNN ($f_{\pi NN} = 1$) and axial ($g_A = 1.26$) couplings, and the form factors (F_1^V, F_ρ) have been taken from the pion production amplitudes of [33].

The Pion-in-flight current corresponding to diagram (c) is purely vector and is given by

$$j^\mu_\pi = \left[I^\pm_V\right]_{1'2',12} \frac{f^2_{\pi NN}}{m^2_\pi} \frac{F_1^V(Q^2)\,\left(k_1^\mu - k_2^\mu\right)}{\left(k_1^2 - m_\pi^2\right)\left(k_2^2 - m_\pi^2\right)} \times \bar u_{s'_1}(\mathbf{p}'_1)\,\gamma_5 \not{k}_1\, u_{s_1}(\mathbf{h}_1) \bar u_{s'_2}(\mathbf{p}'_2)\,\gamma_5 \not{k}_2\, u_{s_2}(\mathbf{h}_2)\,, \tag{15}$$

where $k_2^\mu = (p'_2 - h_2)^\mu$ is the momentum of the pion absorbed by the second nucleon.

The pion-pole current corresponds to diagrams (d,e) and is purely axial, given by

$$j^\mu_{\rm pole} = \left[I^\pm_V\right]_{1'2',12} \frac{f^2_{\pi NN}}{m^2_\pi} \frac{F_\rho\left(k_1^2\right)}{g_A}\, Q^\mu \bar u_{s'_1}(\mathbf{p}'_1) \not{Q} u_{s_1}(\mathbf{h}_1) \times \frac{\bar u_{s'_2}(\mathbf{p}'_2)\,\gamma_5 \not{k}_2\, u_{s_2}(\mathbf{h}_2)}{\left(k_2^2 - m_\pi^2\right)\left(Q^2 - m_\pi^2\right)} + (1\leftrightarrow 2)\,. \tag{16}$$

Finally the Δ current corresponds in Fig. 1 to diagrams (f, g) for the forward and (h, i) for the backward Δ propagations, respectively. The current matrix elements are given by

$$j^\mu_\Delta = j^\mu_{\Delta,\rm F} + j^\mu_{\Delta,\rm B} \tag{17}$$

$$j^\mu_{\Delta,\rm F} = \frac{f^* f_{\pi NN}}{m^2_\pi}\left[U^\pm_{\rm F}\right]_{1'2',12} \frac{\bar u_{s'_2}(\mathbf{p}'_2)\,\gamma_5 \not{k}_2\, u_{s_2}(\mathbf{h}_2)}{k_2^2 - m_\pi^2} \times k_2^\alpha\, \bar u_{s'_1}(\mathbf{p}'_1) G_{\alpha\beta}(h_1 + Q)\Gamma^{\beta\mu}(h_1, Q) u_{s_1}(\mathbf{h}_1) + (1\leftrightarrow 2) \tag{18}$$

$$j^\mu_{\Delta,\rm B} = \frac{f^* f_{\pi NN}}{m^2_\pi}\left[U^\pm_{\rm B}\right]_{1'2',12} \frac{\bar u_{s'_2}(\mathbf{p}'_2)\,\gamma_5 \not{k}_2\, u_{s_2}(\mathbf{h}_2)}{k_2^2 - m_\pi^2} \times k_2^\beta\, \bar u_{s'_1}(\mathbf{p}'_1) \hat\Gamma^{\mu\alpha}(p'_1, Q) G_{\alpha\beta}(p'_1 - Q) u_{s_1}(\mathbf{h}_1) + (1\leftrightarrow 2)\,. \tag{19}$$

The $\pi N\Delta$ coupling is $f^* = 2.13$. The forward, $U^\pm_{\rm F} = U_{Fx} \pm iU_{Fy}$, and backward, $U^\pm_{\rm B} = U_{Bx} \pm iU_{By}$, isospin transition operators have the following Cartesian components

$$U_{\rm Fj} = \sqrt{\frac{3}{2}} \sum_i \left(T_i T_j^\dagger\right) \otimes \tau_i \tag{20}$$

$$U_{\rm Bj} = \sqrt{\frac{3}{2}} \sum_i \left(T_j T_i^\dagger\right) \otimes \tau_i, \tag{21}$$

where $\vec T$ and $\vec T^\dagger$ are the isovector transition operators from isospin $\frac{3}{2}$ to $\frac{1}{2}$ or vice-versa, respectively. The $+(-)$ operator is for neutrino (antineutrino) scattering.

The Δ-propagator, $G_{\alpha\beta}(P)$, is given by

$$G_{\alpha\beta}(P) = \frac{\mathcal{P}_{\alpha\beta}(P)}{P^2 - M_\Delta^2 + iM_\Delta\Gamma_\Delta + \frac{\Gamma_\Delta^2}{4}}\,, \tag{22}$$

where $\mathcal{P}_{\alpha\beta}(P)$ is the projector over spin-$\frac{3}{2}$ on-shell particles,

$$\mathcal{P}_{\alpha\beta}(P) = -(\not{P} + M_\Delta)\left[g_{\alpha\beta} - \frac{1}{3}\gamma_\alpha\gamma_\beta - \frac{2}{3}\frac{P_\alpha P_\beta}{M_\Delta^2} + \frac{1}{3}\frac{P_\alpha\gamma_\beta - P_\beta\gamma_\alpha}{M_\Delta}\right] \tag{23}$$

and whose denominator has been obtained from the free propagator for stable particles, $\frac{1}{P^2 - M_\Delta^2}$, with the replacement $M_\Delta \to$

$M_\Delta - i\frac{\Gamma_\Delta}{2}$ to take into account the finite decay width of the $\Delta(1232)$.

The tensor $\Gamma^{\beta\mu}(P,Q)$ in the forward current is the weak $N \to \Delta$ transition vertex – a combination of gamma matrices with vector and axial-vector contributions:

$$\Gamma^{\beta\mu}(P,Q) = \Gamma_V^{\beta\mu}(P,Q) + \Gamma_A^{\beta\mu}(P,Q) \tag{24}$$

$$\begin{aligned}\Gamma_V^{\beta\mu}(P,Q) = \Bigg[& \frac{C_3^V}{m_N}\left(g^{\beta\mu}\not{Q} - Q^\beta\gamma^\mu\right) \\ & + \frac{C_4^V}{m_N^2}\left(g^{\beta\mu}\,Q\cdot(P+Q) - Q^\beta(P+Q)^\mu\right) \\ & + \frac{C_5^V}{m_N^2}\left(g^{\beta\mu}\,Q\cdot P - Q^\beta P^\mu\right) + C_6^V g^{\beta\mu}\Bigg]\gamma_5\end{aligned} \tag{25}$$

$$\begin{aligned}\Gamma_A^{\beta\mu}(P,Q) = & \frac{C_3^A}{m_N}\left(g^{\beta\mu}\not{Q} - Q^\beta\gamma^\mu\right) \\ & + \frac{C_4^A}{m_N^2}\left(g^{\beta\mu}\,Q\cdot(P+Q) - Q^\beta(P+Q)^\mu\right) \\ & + C_5^A g^{\beta\mu} + \frac{C_6^A}{m_N^2}Q^\beta Q^\mu\,.\end{aligned} \tag{26}$$

For the backward current, we take

$$\hat{\Gamma}^{\mu\alpha}(P',Q) = \gamma^0\left[\Gamma^{\alpha\mu}(P',-Q)\right]^\dagger\gamma^0\,. \tag{27}$$

Finally, it is worth noting that the form factors $C_i^{V,A}$ are taken from [33]. We refer to that work for further details of the model.

2.4. The frozen Δ-propagator

The evaluation of the relevant elementary responses requires one to contract the electroweak two-body MEC with themselves by spin–isospin summation. This leads to the squares of each of the diagrams depicted in Fig. 1 plus all their interferences.

The validity of the frozen nucleon approximation relies on the fact that the integrand inside the 2p–2h response is a function that depends slowly on the momenta of the two initial nucleons inside the Fermi sea. In that case the mean-value theorem applied to the resolution of the integrals provides very precise results. This is so for all of the diagrams of the MEC except for the forward Δ diagram, which shows a sharp maximum for kinematics around the Δ peak for pion emission, located at $\omega = \sqrt{q^2 + m_\Delta^2} - m_N$. This is due to the denominator in the Δ propagator,

$$G_\Delta(H+Q) \equiv \frac{1}{(H+Q)^2 - M_\Delta^2 + iM_\Delta\Gamma_\Delta + \frac{\Gamma_\Delta^2}{4}}\,, \tag{28}$$

where $H^\mu = (E_{\mathbf{h}}, \mathbf{h})$ is the momentum of the hole that gets excited to a Δ.

In these cases the integrand changes very significantly with a small variation of the momentum of the holes and consequently, the frozen approximation cannot properly describe the integrand. On the contrary, it only provides a general estimation of the order of magnitude. To get rid of these difficulties we have developed a prescription to deal with the forward Δ-propagator appearing in Eq. (18). This procedure is based on the use of an effective propagator ("frozen") for the Δ, conveniently averaged over the Fermi gas. This average is an analytical complex function, which is used instead of the "bare" propagator inside the frozen approximation, recovering the precision of the rest of diagrams.

The "frozen" prescription amounts to the replacement:

$$G_\Delta(H+Q) \to G_{\text{frozen}}(Q)\,, \tag{29}$$

where the frozen denominator is defined by

$$G_{\text{frozen}}(Q) = \frac{\int d^3h\,\theta(k_F - |\mathbf{h}|)\,G_\Delta(H+Q)}{\frac{4}{3}\pi k_F^3}\,. \tag{30}$$

Taking the non-relativistic limit for the energies of the holes ($E_{\mathbf{h}} \simeq m_N$), which is justified because hole momenta are below the Fermi momentum, itself a value far below the nucleon rest mass, we can write:

$$G_{\text{frozen}}(Q) = \frac{1}{\frac{4}{3}\pi k_F^3}\int \frac{d^3h\,\theta(k_F - |\mathbf{h}|)}{a - 2\,\mathbf{h}\cdot\mathbf{q} + ib}\,, \tag{31}$$

where

$$a \equiv m_N^2 + Q^2 + 2m_N\omega - M_\Delta^2 + \frac{\Gamma_\Delta^2}{4} \tag{32}$$

$$b \equiv M_\Delta\Gamma_\Delta\,. \tag{33}$$

Assuming the Δ width (Γ_Δ) to be constant, we can integrate Eq. (31) over the angles, getting

$$G_{\text{frozen}}(Q) = \frac{1}{\frac{4}{3}\pi k_F^3}\frac{\pi}{q}\int_0^{k_F} dh\,h\ln\left[\frac{a + 2hq + ib}{a - 2hq + ib}\right]. \tag{34}$$

Note the complex logarithm inside the integral, which provides the needed kinematical dependence of the averaged propagator, differing from the bare Lorentzian shape. Finally the integral over the momentum h can also be performed, resulting in

$$\begin{aligned}G_{\text{frozen}}(Q) = \frac{1}{\frac{4}{3}\pi k_F^3}\frac{\pi}{q}\Bigg\{ & \frac{(a+ib)\,k_F}{2q} \\ & + \frac{4q^2k_F^2 - (a+ib)^2}{8q^2}\ln\left[\frac{a + 2k_Fq + ib}{a - 2k_Fq + ib}\right]\Bigg\}\,.\end{aligned} \tag{35}$$

By comparing the response functions evaluated in the frozen approximation, *i.e.,* substituting the denominator of the Δ propagator in Eq. (22) for the frozen expression in Eq. (35), with the exact results, we find that the shapes around the Δ peak are similar, but with slightly different width and position of the center of the peak. We have checked that the differences can be minimized by changing the parameters a, b with respect to the "bare" ones, given by Eqs. (32), (33). This is because we have computed the averaged denominator without taking into account the current matrix elements appearing in the exact responses, although the functional form and kinematical dependence is the appropriate one.

In practice, we adjust Γ_Δ and apply a shift in the expression for a in Eq. (32) in order to obtain the best approximation to the exact results. The effective "frozen" parameters we actually introduce in Eq. (35), are given by

$$a_{\text{frozen}} \equiv m_N^2 + Q^2 + 2m_N(\omega + \Sigma_{\text{frozen}}) - M_\Delta^2 + \frac{\Gamma_{\text{frozen}}^2}{4} \tag{36}$$

$$b_{\text{frozen}} \equiv M_\Delta\Gamma_{\text{frozen}}\,. \tag{37}$$

We consider Γ_{frozen} and the frozen shift, Σ_{frozen}, to be tunable parameters depending on the momentum transfer q. We have adjusted these parameters for different q-values and we provide them in Table 1.

Table 1
Values of the free parameters of the Fermi-averaged Δ-propagator for different kinematic situations corresponding to different values of the momentum transfer q.

q (MeV/c)	Σ_{frozen} (MeV)	Γ_{frozen} (MeV)
300	20	130
400	65	147
500	65	145
800	80	125
1000	100	100
1200	115	85
1500	150	40
2000	150	0

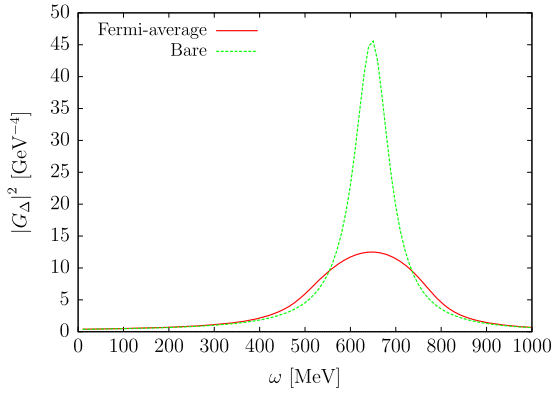

Fig. 2. (Color online.) Square of the absolute value of the spin-independent term of the Δ-propagator in frozen approximation compared to the average propagator. In this evaluation we have taken $q = 1000$ MeV/c and $\Gamma_\Delta = 120$ MeV.

3. Results

In this section we validate the frozen approximation by computing the approximate 2p–2h response functions and comparing with the exact results in the RFG. We consider the case of the nucleus ^{12}C with Fermi momentum $k_F = 225$ MeV/c, and show the different response functions for low to high values of the momentum transfer. For other nuclei with different k_F the frozen parameters of Table 1 should be determined again, and we expect their values change slightly.

In Fig. 2 we show the modulus squared of the Δ propagator, given by the $G_\Delta(H+Q)$ function defined in Eq. (28), computed for $\mathbf{h} = 0$, as a function of ω for $q = 1$ GeV/c. It presents the typical Lorentzian shape corresponding to width $\Gamma_\Delta = 120$ MeV. We observe a narrow peak around $\omega \simeq 650$ MeV. This corresponds to the Δ-peak position for $q = 1$ GeV/c. In the same figure we also show the square of the frozen average G_{frozen} (solid line). The resulting peak is quenched and broadened as compared to the Lorentzian shape, reducing its strength and enlarging its width. This behavior of the averaged Δ-propagator drives the actual shape of the exact 2p–2h nuclear responses, being more realistic than the simple Lorentzian shape of the frozen approximation without the average, as we will see below.

In Fig. 3 we show the weak transverse 2p–2h response function of ^{12}C for four different values of the momentum transfer ranging from 300 to 1500 MeV/c. The curves correspond to different calculations or approximations made in the evaluation of the responses, as labeled in the legend. The solid line corresponds to the seven-dimensional calculation with no approximations. The other two curves refer to the different frozen nucleon approximations developed in this work: the dashed line is obtained with Eq. (12) but performing the replacement expressed in (30) for the forward Δ-excitation terms in the evaluation of the current matrix elements; on the contrary, the dotted line corresponds to the same

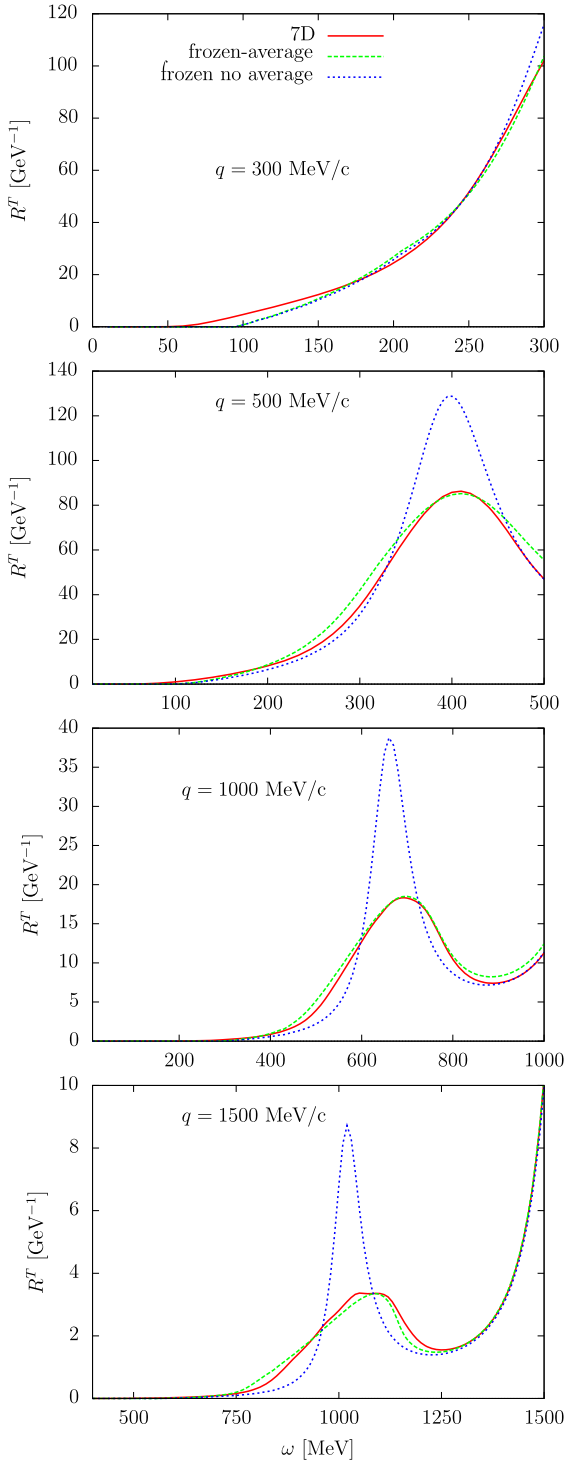

Fig. 3. (Color online.) 2p–2h transverse response function R^T of ^{12}C for different momentum transfers q. The exact results are compared to the frozen approximation with and without the averaged Δ propagator.

frozen nucleon approximation, Eq. (12), but without the Fermi-average of the Δ-propagator in the forward terms.

As it can be seen from Fig. 3, for those values of the momentum transfer for which the Δ-peak is not reached (the panel with $q = 300$ MeV/c), there is really little difference between averaging or not the Δ propagator. This is certainly not the case when the Δ-peak is fully reached, as shown in the other panels. In this situation there is a dramatic difference between performing the

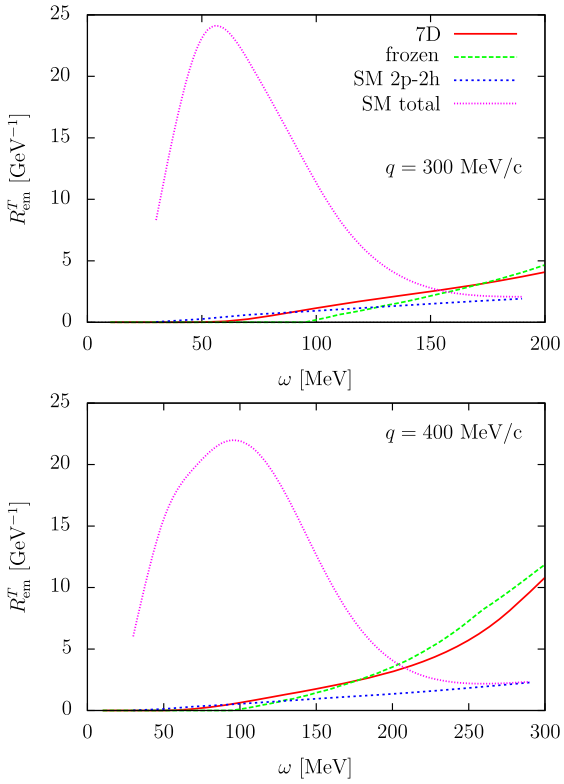

Fig. 4. (Color online.) Comparison of 2p–2h electromagnetic transverse response functions of ^{12}C within different models for two values of the momentum transfer. The exact RFG results and the frozen approximation are compared with the shell model (SM) results of [34]. The total shell model results (1p–1h) + (2p–2h) are also shown for comparison.

Fermi-average of the Δ-propagator or not. This difference is in consonance with the results shown in the previous Fig. 2, and it shows how crucial is the treatment of the Δ-propagator to obtain accurate results for the 2p–2h responses in the frozen nucleon approximation, i.e, with only one integration.

The results in Fig. 3 have been obtained after fitting the parameters ($\Delta_{\rm frozen}$, $\Gamma_{\rm frozen}$) for the Fermi-averaged Δ-propagator at the different values of the momentum transfer quoted in Table 1. It is also worth noting that there is no way of converting the dotted line into the dashed one by only a suitable fitting of these parameters, *i.e.,* without averaging the Δ-propagator.

In Fig. 4 we show results for the transverse electromagnetic 2p–2h response function. The frozen and exact (7D) T response of the RFG are compared with the results obtained in the shell model 2p–2h calculation of [34]. This was one of the first computations of the 2p–2h response within the nuclear shell model. The total nuclear response in the shell model, obtained by adding the 1p–1h to the 2p–2h channel, is also shown to appreciate the relative size of the 2p–2h contribution to the total result.

As shown in Fig. 4, the Fermi gas results (either in frozen approximation or not) are similar to the shell model ones. The small discrepancy for $q = 300$ MeV/c between them cannot be attributed to relativistic effects because of the low momentum transfer value considered, but to the different coupling constants and form factors used in the model of the Δ meson-exchange current considered in [34] and the present approach. For $q = 400$ MeV/c the larger discrepancy, starting from $\omega = 250$ MeV, can be attributed to the dynamic treatment of the Δ propagator in the relativistic case, while in the shell model the Δ propagator is static. We can remark the slightly different threshold effects between both calculations. These effects are, as expected, very sensitive to the

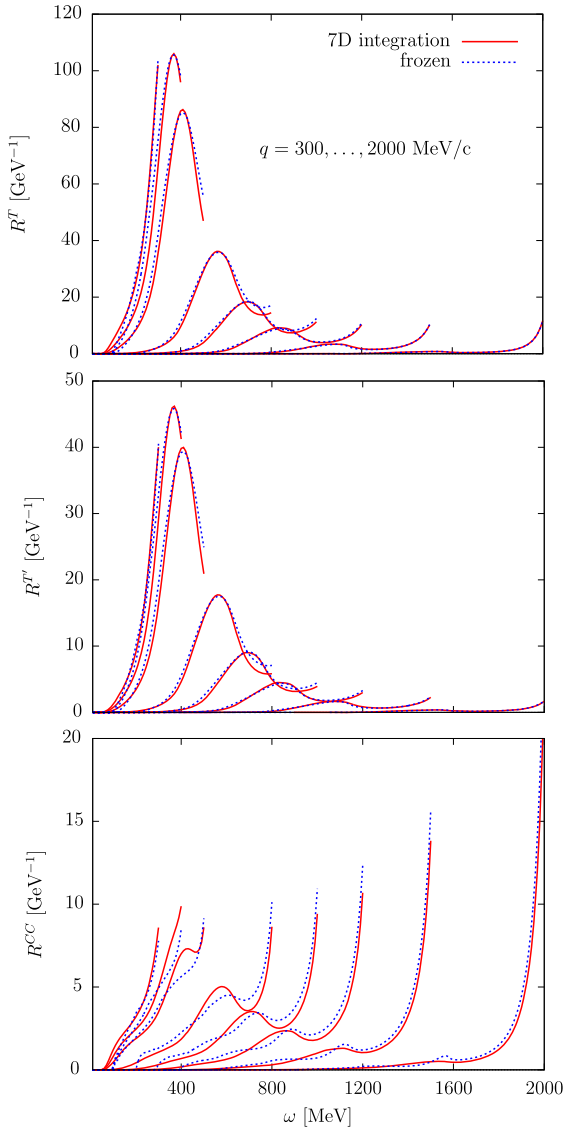

Fig. 5. (Color online.) Comparison of the frozen approximation with the exact results for several 2p–2h CC weak response functions. The target is ^{12}C. Several values of the momentum transfer are displayed: $q = 300, 400, 500, 1000, 1200, 1500$ and 2000 MeV/c.

treatment of the nuclear ground state. Note also that the frozen approximation describes reasonably well this low momentum $q =$ 300 MeV/c, considering the simplifications involved.

Finally in Fig. 5 we show that the frozen approximation works notably well in a range of momentum transfer from low to high values of q. We compare the T, T', and CC 2p–2h responses in frozen approximation with the exact results obtained computing numerically the 7D integral of the hadronic tensor. The accord is particularly good for the two transverse responses which dominate the cross section. A slight disagreement occurs for very low energy transfer at threshold where the response functions are anyway small. In the case of the CC response function some tiny differences are observed. However, note that this response is small because the dominant Δ current is predominantly transverse. Moreover, its global contribution to the cross section is not very significant because it is partially canceled with the contribution of the CL and LL responses.

We have checked that the cross section for fixed incident neutrino energy agrees well with the exact results, as expected, be-

cause it is computed as a linear combination of the five response functions with a greater contribution from the T and T' ones. In a real experimental situation an integration over the incident neutrino flux is needed. This flux integration has been performed in [37] by using a parametrization of the exact results of the present model, with a good global agreement with the experimental data. We refer to [37] for the numerical results. In this work we have shown that this can also be done within the frozen approximation as an alternative with similar results.

Physical interpretation of the frozen approximation. The validity of the frozen approximation led us to conclude that, in the inclusive responses for two-particle emission, the detailed information about the momenta carried out by the two nucleons is lost. This is because the energy and momentum transfer ω, q are shared by the two nucleons in multiple ways. This is reminiscent from the phase-space kinematical dependence (which can be obtained setting the elementary response r^K to unity) already seen in [29]. The soft dependence of the elementary response on the initial momenta makes the same argument applicable to the full responses with the exception of the Δ forward current that requires one to soften and average the rapid variations of the Δ propagator. Only the low-energy region where the sharing is highly restricted and the cross section is therefore very small, is found to be sensitive to the details of the initial state. This is also supported by the comparison between the shell model and the RFG.

Finally, it is interesting to explicitly quantify the computational time gain of the frozen approximation. For a typical numerical integration with ten points per dimension one roughly expects a reduction factor $\sim 10^6$. On an average laptop the CPU time for computing the five response functions at a given (q, ω) point is about 0.01 s, while the full calculation takes about 3 h.

4. Conclusions

In this work we have introduced and validated the frozen nucleon approximation for a fast and precise calculation of the inclusive 2p–2h response functions in a relativistic Fermi gas model. This approximation neglects the momentum dependence of the two holes in the ground state and requires the use of an effective propagator for the Δ resonance conveniently averaged over the Fermi sphere, for which we have provided a simple analytical expression. For momentum transfers above the Fermi momentum this approximation makes it possible to compute the responses with only a one-dimensional integral. Taking into account all the uncertainties in modeling the two-nucleon emission reactions, this approach can be used instead of the full 7D integral, obtaining very satisfactory results. Although we have used a specific model of MEC to prove the validity of the approximation, it is reasonable to expect that the frozen approach is also valid for other 2p–2h models [3,4,6,8,9,35,36]. This can be of great interest when implementing 2p–2h models in Monte Carlo event generators, which up to now have relied on parameterizations from external calculations. In summary, the frozen approximation enables one to make 2p–2h calculations very efficiently and rapidly, instead of interpolating pre-calculated tables, including allowing the parameters of the models to be modified inside the codes, if desired. Finally, in the near future this study will be extended to an exploration of how the 2p–2h MEC responses depend on nuclear species [38].

Acknowledgements

This work has been partially supported by the Spanish Ministerio de Economía y Competitividad (grant Nos. FIS2014-559386-P and FIS2014-53448-C2-1 and ERDF (European Regional Development Fund) under contracts FIS2014-59386-P, FIS2014-53448-C2-1, by the Junta de Andalucia (grants No. FQM-225, FQM160), by the INFN under project MANYBODY, and part (TWD) by the U.S. Department of Energy under cooperative agreement DE-FC02-94ER40818. IRS acknowledges support from a Juan de la Cierva fellowship from MINECO (Spain). GDM acknowledges support from a Junta de Andalucia fellowship (FQM7632, Proyectos de Excelencia 2011).

References

[1] U. Mosel, Annu. Rev. Nucl. Part. Sci. 66 (2016) 1–26.
[2] T. Katori, M. Martini, arXiv:1611.07770 [hep-ph].
[3] M. Martini, M. Ericson, G. Chanfray, J. Marteau, Phys. Rev. C 80 (2009) 065501.
[4] M. Martini, M. Ericson, G. Chanfray, J. Marteau, Phys. Rev. C 81 (2010) 045502.
[5] J.E. Amaro, M.B. Barbaro, J.A. Caballero, T.W. Donnelly, C.F. Williamson, Phys. Lett. B 696 (2011) 151.
[6] J. Nieves, I. Ruiz Simo, M.J. Vicente Vacas, Phys. Rev. C 83 (2011) 045501.
[7] J.E. Amaro, M.B. Barbaro, J.A. Caballero, T.W. Donnelly, Phys. Rev. Lett. 108 (2012) 152501.
[8] J. Nieves, I. Ruiz Simo, M.J. Vicente Vacas, Phys. Lett. B 707 (2012) 72.
[9] R. Gran, J. Nieves, F. Sanchez, M.J. Vicente Vacas, Phys. Rev. D 88 (2013) 113007.
[10] A.A. Aguilar-Arevalo, et al., MiniBooNE Collaboration, Phys. Rev. D 81 (2010) 092005.
[11] Y. Nakajima, et al., SciBooNE Collaboration, Phys. Rev. D 83 (2011) 012005.
[12] C. Anderson, et al., ArgoNeuT Collaboration, Phys. Rev. Lett. 108 (2012) 161802.
[13] K. Abe, et al., T2K Collaboration, Phys. Rev. D 87 (9) (2013) 092003.
[14] G.A. Fiorentini, et al., MINERvA Collaboration, Phys. Rev. Lett. 111 (2013) 022502.
[15] K. Abe, et al., T2K Collaboration, Phys. Rev. D 90 (5) (2014) 052010.
[16] T. Walton, et al., MINERvA Collaboration, Phys. Rev. D 91 (7) (2015) 071301.
[17] A.M. Ankowski, O. Benhar, C. Mariani, E. Vagnoni, Phys. Rev. D 93 (2016) 113004.
[18] P.A. Rodrigues, et al., MINERvA Collaboration, Phys. Rev. Lett. 116 (2016) 071802.
[19] K. Abe, et al., T2K Collaboration, Phys. Rev. D 93 (2016) 112012.
[20] Y. Hayato, Acta Phys. Pol. B 40 (2009) 2477.
[21] C. Andreopoulos, GENIE Collaboration, Acta Phys. Pol. B 40 (2009) 2461.
[22] C. Andreopoulos, et al., Nucl. Instrum. Methods A 614 (2010) 87.
[23] J. Sobczyk, PoS NUFACT 08 (2008) 141.
[24] J. Schwehr, D. Cherdack, R. Gran, arXiv:1601.02038 [hep-ph].
[25] J. Żmuda, K.M. Graczyk, C. Juszczak, J.T. Sobczyk, Acta Phys. Pol. B 46 (11) (2015) 2329.
[26] C. Wilkinson, et al., Phys. Rev. D 93 (2016) 072010.
[27] A. Bodek, H.S. Budd, M.E. Christy, Eur. Phys. J. C 71 (2011) 1726.
[28] J.W. Van Orden, T.W. Donnelly, Ann. Phys. 131 (1981) 451.
[29] I. Ruiz Simo, C. Albertus, J.E. Amaro, M.B. Barbaro, J.A. Caballero, T.W. Donnelly, Phys. Rev. D 90 (3) (2014) 033012.
[30] I. Ruiz Simo, J.E. Amaro, M.B. Barbaro, A. De Pace, J.A. Caballero, T.W. Donnelly, J. Phys. G: Nucl. Part. Phys. 44 (2017) 065105.
[31] J.E. Amaro, M.B. Barbaro, J.A. Caballero, T.W. Donnelly, C. Maieron, Phys. Rev. C 71 (2005) 065501.
[32] I. Ruiz Simo, C. Albertus, J.E. Amaro, M.B. Barbaro, J.A. Caballero, T.W. Donnelly, Phys. Rev. D 90 (5) (2014) 053010.
[33] E. Hernandez, J. Nieves, M. Valverde, Phys. Rev. D 76 (2007) 033005.
[34] J.E. Amaro, A.M. Lallena, G. Co, Nucl. Phys. A 578 (1994) 365.
[35] T. Van Cuyck, N. Jachowicz, R. Gonzalez-Jimenez, M. Martini, V. Pandey, J. Ryckebusch, N. Van Dessel, Phys. Rev. C 94 (2) (2016) 024611.
[36] T. Van Cuyck, N. Jachowicz, R. Gonzalez-Jimenez, J. Ryckebusch, N. Van Dessel, arXiv:1702.06402 [nucl-th].
[37] G.D. Megias, J.E. Amaro, M.B. Barbaro, J.A. Caballero, T.W. Donnelly, I. Ruiz Simo, Phys. Rev. D 94 (2016) 093004.
[38] J.E. Amaro, M.B. Barbaro, J.A. Caballero, A. De Pace, T.W. Donnelly, G.D. Megias, I. Ruiz Simo, arXiv:1704.01539 [nucl-th].